A versatile and easy method to calibrate a two-compartment flow cell for differential electrochemical mass spectrometry measurements

Bondue, C.J.; Koper, M.T.M.; Tschulik, K.

ACS MEASUREMENT SCIENCE Au
AN OPEN ACCESS JOURNAL OF THE AMERICAN CHEMICAL SOCIETY

pubs.acs.org/measureau

Article

A Versatile and Easy Method to Calibrate a Two-Compartment Flow Cell for Differential Electrochemical Mass Spectrometry Measurements

Christoph J. Bondue, Marc T. M. Koper, and Kristina Tschulik*

Cite This: ACS Meas. Sci. Au 2023, 3, 277−286

Read Online

ACCESS | Metrics & More | Article Recommendations | Supporting Information

ABSTRACT: Online techniques for the quantitative analysis of reaction products have many advantages over offline methods. However, owing to the low product formation rates in electrochemical reactions, few of these techniques can be coupled to electrochemistry. An exception is differential electrochemical mass spectrometry (DEMS), which gains increasing popularity not least because of its high time resolution in the sub-second regime. DEMS is often combined with a dual thin-layer cell (a two-compartment flow cell), which helps to mitigate a number of problems that arise due to the existence of a vacuum|electrolyte interface. However, the efficiency with which this cell transfers volatile reaction products into the vacuum of the mass spectrometer is far below 100%. Therefore, a calibration constant that considers not only the sensitivity of the DEMS setup but also the transfer efficiency of the dual thin-layer cell is needed to translate the signals observed in the mass spectrometer into electrochemical product formation rates. However, it can be challenging or impossible to design an experiment that yields such a calibration constant. Here, we show that the transfer efficiency of the dual thin-layer cell depends on the diffusion coefficient of the analyte. Based on this observation, we suggest a two-point calibration method. That is, a plot of the logarithm of the transfer efficiencies determined for H_2 and O_2 versus the logarithm of their diffusion coefficients defines a straight line. Extrapolation of this line to the diffusion coefficient of another analyte yields a good estimate of its transfer efficiency. This is a versatile and easy calibration method, because the transfer efficiencies of H_2 and O_2 are readily accessible for a large range of electrode−electrolyte combinations.

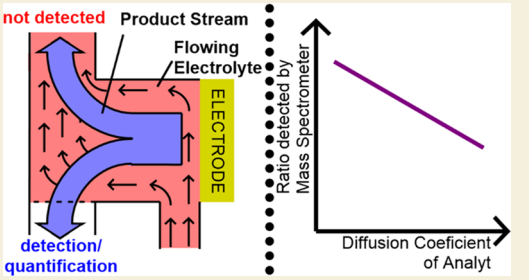

KEYWORDS: *differential electrochemical mass spectrometry, dual thin-layer cell, flow cell, calibration, electrochemical alcohol oxidation*

INTRODUCTION

Differential electrochemical mass spectrometry (DEMS) is an experimental technique that allows the detection of volatile products formed during electrochemical reactions by mass spectrometric means. This renders DEMS a very useful tool in the study of reaction mechanisms such as the reduction of nitrate,[1] the competition between hydrogen evolution and CO_2 reduction,[2] and the selective reduction of ethyne to ethene.[3] However, the presence of a vacuum|liquid electrolyte interface, which is inherent to the DEMS technique, complicates the study of these reactions, as they involve either the formation of a volatile intermediate (nitrate reduction) or volatile reactants (CO_2 and ethyne reduction). In arrangements in which the electrochemical reaction proceeds directly at the vacuum|electrolyte interface or in its immediate proximity, a mass transport competition between electrode and vacuum|electrolyte interface arises.[1,4] Hence, the working electrode is either starved of the reactant[4] or reaction intermediates are removed from the electrode before they react further.[1] In both cases, the measurement interferes with the product distribution of the electrochemical reaction, a situation that must be avoided to gain meaningful information about the electrochemical system under investigation. We do not expect that this issue is fixed when the vacuum|electrolyte interface is substituted for an interface between electrolyte and carrier gas as in the SNIFFER chip.[5] That is, the relevant quantity is the partial pressure of the analyte (and not the absolute pressure) that must be kept low to achieve diffusion limited transfer of the analyte into the gas phase. This is a precondition for the use of DEMS as a quantitative technique, because only then do the amounts of evaporated analyte and therefore the signal detected by the mass spectrometer reflect on the formation rate of the analyte. Otherwise, the signal intensity would be convoluted by the kinetics or the thermodynamics of the evaporation process, yielding qualitative information only.

Received: March 9, 2023
Revised: May 8, 2023
Accepted: May 8, 2023
Published: May 19, 2023

It stands therefore to reason that mass transport competition will always arise when the electrode is immediately placed at the interface between the electrolyte and the gas phase. This issue can be overcome,[4] when the dual thin-layer cell is used, which was first introduced by Jusys et al.[6] In this cell, the electrochemical formation of volatile reaction products proceeds in a different location than their transfer into the vacuum of the mass spectrometer.[6,7] Constant electrolyte flow through the cell transports the volatile reaction products along with the electrolyte to the vacuum|electrolyte interface. Other flow cells[8−11] or the bead-crystal flow-through cell,[12,13] and what appears to be an adaptation of it,[14,15] can be expected to avoid the negative effect of the vacuum|electrolyte interface as well. However, all these cells are likely to suffer from the same drawback as the dual thin-layer cell: The efficiency with which a flow cell transfers volatile reaction products into the vacuum of the mass spectrometer is usually far below 100%.[7] This poses a problem when one desires to translate the signal, detected by the mass spectrometer, into an electrochemical product formation rate. The issue is comparable to a rotating ring disc electrode (RRDE) experiment: A product molecule that is detected at the ring electrode represents several more product molecules that travel from the center electrode outward to the bulk electrolyte without undergoing a reaction. Therefore, a collection efficiency must be considered when the current at the ring electrode is interpreted as product formation rate at the disc electrode. The transfer efficiency of a flow cell in a DEMS experiment has the same function as the collection efficiency in an RRDE experiment. Hence, quantification of the mass spectrometric signal requires a calibration constant that considers both the overall sensitivity of the DEMS setup and the transfer efficiency of the flow cell.[7] So far, it was only possible to determine such a calibration constant from a DEMS experiment in which the analyte is either formed or consumed in an electrochemical reaction of known Faradaic efficiency. In this case, the formed (or consumed) amount of analyte can be determined from the charge that is passed during the electrochemical reaction. A calibration constant is obtained, when the amount of electrochemically formed products is related to the signal observed by the mass spectrometer. The calibration constant obtained in this way comprises both the transfer efficiency of the dual thin-layer cell and the sensitivity of the DEMS setup.[7] This procedure has to be repeated every time the cell is set up anew, because the exact cell geometry and therefore the transfer efficiency change with each setting up. For this reason, it is only possible to change the electrolyte, but not the electrode, to create conditions under which the analyte is formed (or consumed) with known Faradaic efficiency. This is often a difficult condition to meet, and it can become daunting or impossible to calibrate the dual thin-layer cell or any other flow cell.

In this work, we show that the transfer efficiency of the dual thin-layer cell depends on the diffusion coefficient of the analyte. Based on this observation, we suggest a two-point calibration method. That is, a plot of the logarithm of the transfer efficiencies determined for H_2 and O_2 versus the logarithm of their diffusion coefficients defines a straight line. The transfer efficiency of another compound can then be determined by extrapolation to its diffusion coefficient. Since the transfer efficiencies of H_2 and O_2 are usually readily accessible for aqueous electrolytes, this procedure is an easy-to-use and (almost) universal calibration method.

EXPERIMENTAL SECTION

Chemicals and Materials

Electrolytes were either prepared from $NaClO_4$ (99.99%, trace metal basis, Sigma-Aldrich), $HClO_4$ (60% by wt. solution, EMSURE, Merck), KOH (86.7%, analytical reagent grade, Fisher Scientific), NaOH (>98%, Puriss, Sigma-Aldrich), $Ni(NO_3)_2$ (for analysis, Sigma-Aldrich), $Co(NO_3)_2$ (Puratronic, Alfa Aesar), 2-propanol (Normapur, VWR Chemicals), argon (5.0 purity, Linde), and CO (4.7 purity, Linde).

The dual thin-layer cell was manufactured from PCTFE and constantly purged with argon to keep ambient air from entering the vacuum of the mass spectrometer. This allows a steady base line on masses 32 and 44. A PTFE membrane (PTF002LH0P—Samp, Pall Inc.) was peeled with a scalpel from the support, and two layers of it were used to form the vacuum|electrolyte interface. Four layers of the same PTFE membrane were used as spacers. Electrochemical measurements were conducted either with an Ivium CompactStat or with a PalmSens Potentiostat.

During the experiments, the electrolyte is continuously purged with argon or CO. Hence, the electrolyte should be saturated with the respective gas during the electrochemical experiment.

Electrode Preparation

In order to cover a stainless-steel electrode with a $Co(OH)_2$/$Ni(OH)_2$ codeposit, we followed the procedure outline by Sun and Xu.[16] We conducted chronoamperometry at −0.85 V (vs Ag|AgCl) in an electrolyte that featured 0.07 M $Ni(NO_3)_2$ and 0.03 $Co(NO_3)_2$ until a charge of 1 C was passed. This procedure should yield a $Co(OH)_2$/$Ni(OH)_2$ codeposit with a Ni content of 46%.[16] However, no further characterization of the composition was conducted.

DEMS Measurements

DEMS measurements were conducted on two identical, homebuilt DEMS setups. The design followed the principle outlined by Wolter and Heitbaum.[17] In brief: A PEEK sleeve around the mass spectrometer (QMA 410, Pfeiffer Vacuum) divides the vacuum system into two sections, which allows differential pumping of the mass spectrometer. The section of the vacuum system that features the ion source (cross beam with magnets) is pumped with a turbo molecular pump featuring a pumping speed of 255 L/s (HiPace 300, Pfeiffer Vacuum). The section of the vacuum system that features the secondary electron multiplier and the mass filter is pumped with a turbo molecular pump featuring a pumping speed of 66 L/s (HiPace 80, Pfeiffer Vacuum).

In those experiments where we study the electrochemical oxidation of CO to CO_2, the energy of the electrons emitted from the insource is reduced. Therefore, the cathode potential of the insource is set to −27.5 V. In this way, we can avoid fragmentation of CO_2 and monitor the consumption of CO in the ionic current for mass 28 without interfering contributions from CO_2 fragments.[4] Accordingly, there is no need to correct the signal observed for mass 28. In the experiments where we study the oxidation of 2-propanol, the cathode potential is set to −70 V.

Leakage calibration was conducted as outlined by Wolter and Heitbaum.[17] A cavity of known volume is filled with the analyte gas to a pressure of approximately 300 Pa and then leaked gradually into the vacuum of the mass spectrometer. While doing so, a capacitive gauge records the declining pressure in the cavity and the mass spectrometer measures the ionic current for the relevant mass. The ideal gas law is employed to calculate the flux of gas molecules into the mass spectrometer from the decline of the pressure (i.e., the first derivative of the pressure with respect to time) and the volume of the cavity. By relating this flux to the measured ionic current, we can determine $K^{\circ}(x)$, which represents the sensitivity of the DEMS setup for compound x (c.f. eq 1). Leakage calibration for acetone is conducted in the same way. However, in this case, a glass vial is filled with 100 μL of acetone and then placed in the aforementioned cavity. The pressure is then reduced until a value of approximately 300 Pa is reached. All leakage calibration experiments were conducted, while

https://doi.org/10.1021/acsmeasuresciau.3c00009
ACS Meas. Sci. Au 2023, 3, 277−286

Scheme 1[a]

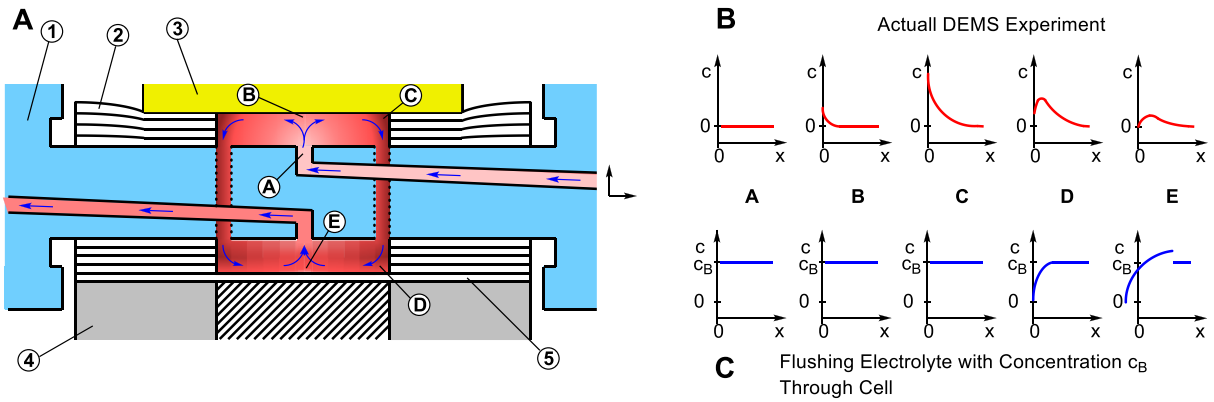

[a]Relevant Part of the Dual Thin-Layer Cell (A). 1: Cell body; 2: PTFE spacer (upper compartment); 3: Working electrode; 4: Steel holder; 5: PTFE membrane (Scheme A: Adapted with Permission under a Creative Commons CC-BY License from Bondue, C. J.; Koper, M. T. *Journal of Electroanalytical Chemistry* 2020, *875* (3), 113, 842. Copyright 2020 Elsevier B.V. The color gradient indicates the evolution of the concentration profile schematically and has not been simulated. (B) Evolution of the concentration profile of the product formed at the electrode in the electrolyte during an electrochemical DEMS Experiment (Positions A, B, C, D and E as indicated in Scheme 1A). (C) Evolution of the concentration profile when an electrolyte featuring the concentration cB of the analyte is flushed through the cell. (B) and (C) Are a simplified representation of the concentration profiles discussed previously.[7,18]

the dual thin-layer cell was flushed with the blank electrolyte and attached to the mass spectrometer. In this way, we can ensure that the partial pressure of water in the ion source is the same during calibration and the actual electrochemical experiment. This is relevant because the presence of water is known to facilitate the detection of the analyte.[19]

RESULTS

Scheme 1A shows a drawing of the relevant parts of the dual thin-layer cell. The working electrode is pressed on rings of PTFE spacers, which leaves a cavity between the working electrode and the cell body. The electrolyte enters the cavity, i.e., the upper compartment, through a capillary in the center and flows along the working electrode toward the outer perimeter of the upper compartment. The electrolyte leaves the upper compartment and enters the lower compartment through six capillaries that are arranged in a circular fashion (only two are shown in Scheme 1). The lower compartment is formed when the cell holder is pressed on the PTFE spacers, which again leaves a cavity between the cell body and the PTFE membrane and leaves the cell through a capillary in the center. Hence, volatile reaction products that accumulate in the electrolyte while flowing along the working electrode can evaporate in the lower compartment when the electrolyte passes the PTFE membrane.

To understand why the dual thin-layer cell has a transfer efficiency of less than 100%, we can consider how the concentration profile evolves within the electrolyte, when it flows from the upper to the lower compartment. This is shown qualitatively in Scheme 1B for different positions in the dual thin-layer cell.[7] When the electrolyte enters the upper compartment in position A, no product is dissolved in the electrolyte. However, formation and, hence, accumulation of the product occur as the electrolyte passes along the working electrode from positions B to C. Mass transport effects cause a profile in which the product concentration is highest at the electrode surface and flattens out in the direction of the cell body. During the transfer of the electrolyte from the upper to the lower compartment, diffusion reduces the concentration gradient (not shown in Scheme 1B). However, a concentration gradient of the product remains when the electrolyte reaches position D unless the diffusion coefficient of the product is very large or the flow rate is very low. The fact that much of the product molecules diffuse in the *x*-direction, when the electrolyte flows from position A to position D, is responsible for a transfer efficiency below 100%: At position D, all molecules that are in the direct proximity of the PTFE membrane evaporate immediately into the vacuum of the mass spectrometer. Hence, the product concentration in the electrolyte closest to the vacuumlelectrolyte interface drops to zero. Accordingly, another concentration gradient emerges that causes some product molecules to diffuse toward the vacuumlelectrolyte interface, while the electrolyte flows along the PTFE membrane from positions D to E. At the same time, product molecules continue to diffuse in the *x*-direction, because a negative concentration gradient in this direction continues to exist. For this reason, the electrolyte will not be depleted completely and a fraction of the electrochemically formed products leave the cell along with the electrolyte, unless the flow rate of the electrolyte is low (and therefore the dwell time in the lower compartment is large). Scheme 1B indicates why a dependence of the transfer efficiency on the diffusion coefficient of the analyte is expected: The shape of the concentration profile and mass transport are related to the diffusion coefficient and determine the fraction of analyte that evaporate at the vacuumlelectrolyte interface. It should also be clear that the transfer efficiency is a function of the electrolyte flow rate through the cell.[7,20] As the latter is increased, the electrolyte spends less time in the lower compartment. Hence, the analyte has less time to diffuse to the membrane and to evaporate into the vacuum of the mass spectrometer. Accordingly, a decrease of the transfer efficiency is observed when the electrolyte flow rate increases.[20]

Sometimes the argument arises that it should be possible to calibrate the dual thin-layer cell by flushing it with an electrolyte that features a known concentration of the analyte. Indeed, considering the electrolyte flow rate and the analyte concentration, it is possible to determine the flux of analyte (in mol/s) through the dual thin-layer cell. However, when the flux of analyte is related to the relevant ionic current, a quantity

https://doi.org/10.1021/acsmeasuresciau.3c00009
ACS Meas. Sci. Au 2023, 3, 277−286

is obtained that does not constitute the transfer efficiency N.[7] This becomes clear from Scheme 1C, which illustrates qualitatively the evolution of the concentration profile when an electrolyte featuring the analyte concentration c_B is flushed through the dual thin-layer cell. Comparison of Scheme 1B and C emphasizes that such an experiment cannot emulate the concentration profile of an actual electrochemical experiment, which is important in determining the transfer efficiency. Hence, only a calibration experiment, in which the same concentration profile arises as in the actual, electrochemical experiment, can yield a calibration constant that accounts for the transfer efficiency.

In order to investigate the dependence of the transfer efficiency on the diffusion coefficient of the analyte, we consider the electrochemical evolution of H_2, O_2, and CO_2 as well as the electrochemical consumption of CO (i.e., oxidation to CO_2) in an electrolyte of 0.5 M $NaClO_4$ containing 10 mM $HClO_4$. Figure 1 shows the CVs and the mass spectrometric

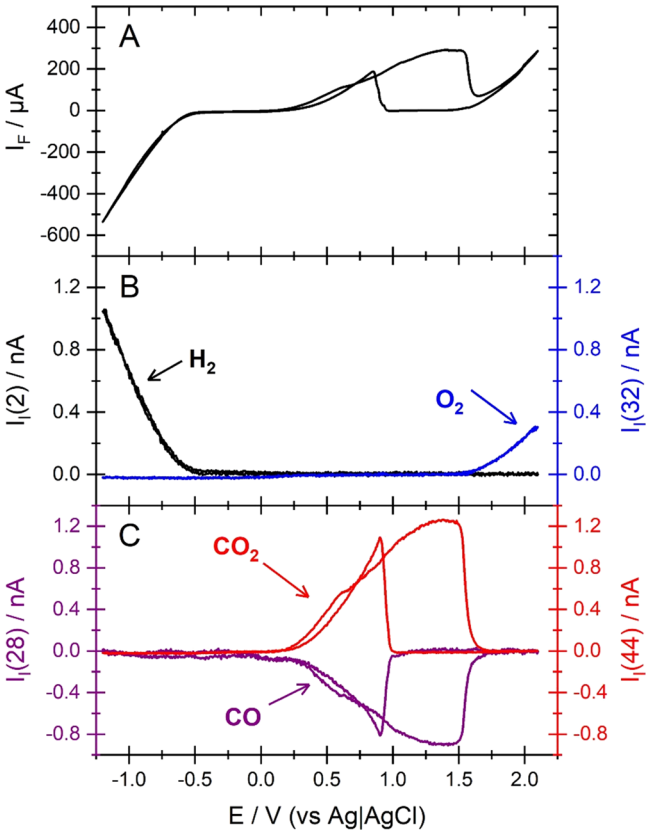

Figure 1. CV (A) and MSCV for masses 2 (black, B), 32 (blue, B), 28 (black, C), and 44 (red, C) obtained during a potential sweep at an Au working electrode in the dual thin-layer cell. Electrolyte: CO saturated 0.5 M $NaClO_4$ + 10 mM $HClO_4$; electrolyte flow rate: 5 µL/s; sweep rate: 20 mV/s. The cathode potential of the ion source of the mass spectrometer was 27.5 V.

CVs (MSCVs) for masses 2, 28, 32, and 44 obtained at a gold electrode. The negative current in the CV and the positive signal in the MSCV for mass 2 indicate the evolution of hydrogen at potentials negative of −0.5 V. Since no CO reduction occurs (absence of a negative ionic current in the MSCV for mass 28), it can be assumed that hydrogen evolution proceeds with 100% Faradaic efficiency. At potentials larger than 0.1 V, the electrochemical oxidation of CO to CO_2 takes place, which can be derived from the negative ionic current in the MSCV for mass 28 (CO consumption) and the positive ionic current in the MSCV for mass 44 (CO_2 formation). Considering the absence of any other electroactive species and the absence of a signal in the MSCV for mass 32 at potentials negative of 1.5 V, it can be assumed that the oxidation of CO to CO_2 occurs with 100% Faradaic efficiency. Note that the presence of 10 mM $HClO_4$ means that neither HCO_3^- nor CO_3^{2-} is stable. As the potential exceeds 1.5 V in the positive going direction, electrochemical CO oxidation stops before electrochemical oxygen evolution sets in. This is indicated by the positive signal in the ionic current for mass 32. Considering that the oxidation of CO has already stopped and that no other electroactive species is present in the electrolyte, it can be assumed that also oxygen evolution proceeds with 100% Faradaic efficiency.

It is therefore possible to employ eq 1

$$I_I(x) = \frac{I_F(x)}{z \cdot F} \cdot N(x) \cdot K^\circ(x) = \frac{I_F(x)}{z \cdot F} \cdot K^*(x) \quad (1)$$

to calculate the calibration constant $K^*(x)$ of compound x from the ionic current $I_I(x)$ (signal of the mass spectrometer) and the Faradaic current $I_F(x)$ (electrochemical current). In eq 1, F is the Faraday constant and z is the number of electrons transferred during the electrochemical reaction. Note that the calibration constant $K^*(x)$ is the product of the transfer efficiency $N(x)$ and $K^\circ(x)$. The latter can be considered the sensitivity of the DEMS system for compound x. Molecular properties such as the ionization cross section and the fragmentation pattern enter this quantity. In the case of H_2, CO, CO_2, and O_2, K° is accessible by the leakage calibration experiment outlined in the Experimental Section.[7,17] Hence, after determination of K^* and determination of K° via leakage calibration, it is possible to determine the transfer efficiency of a given cell setup for H_2, CO, CO_2, and O_2.

To determine the transfer efficiency of H_2, CO, CO_2, and O_2, we have conducted potential step experiments because this allows us to avoid (pseudo)capacitive charging effects that would otherwise add to the Faradaic current. The corresponding experiments are shown in Figure 2−4. In Figure 2 a potential step from 0 to −1 V, in Figure 3 a potential step from 0 to 0.9 V, and in Figure 4 a potential step from 0 to 1.9 V were conducted. Panels A of each of these figures show the measured Faradaic current, and panels B show the corresponding ionic current (Figure 2: mass 2; Figure 3: masses 28 and 44; Figure 4: mass 32). Panels C show the transfer efficiency calculated from the data shown in panels A and B using eq 1. For this, we used the average K° values given in Table 1, which were derived for each gas from the results of four distinct leakage calibration experiments (not shown). Note that the transfer efficiency is constant over time in Figures 2−4, which indicates that bubble formation does not occur in our experiments. The latter would manifest itself in sudden spikes in the ionic current and in the transfer efficiency. These spikes would result from the bursting of bubbles at the membrane, which releases suddenly large quantities of the analyte into the vacuum of the mass spectrometer.

In Figure 5, the logarithm of the transfer efficiency is plotted as the function of the logarithm of the diffusion coefficient (D) of the respective gas. The diffusion coefficients for H_2, O_2, and CO were determined for the employed electrolyte (0.5 M $NaClO_4$ + 10 mM $HClO_4$) by the method introduced by the groups of Fuhrmann and Baltruschat.[18,21] The results of the

https://doi.org/10.1021/acsmeasuresciau.3c00009
ACS Meas. Sci. Au 2023, 3, 277−286

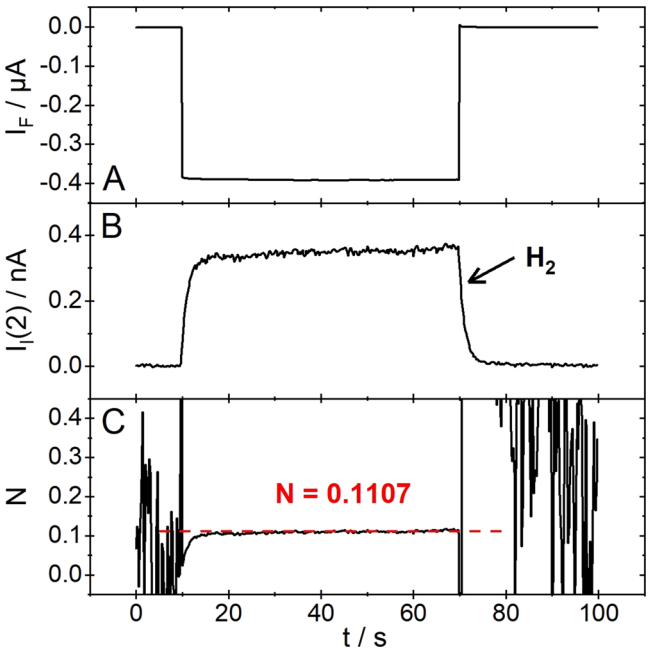

Figure 2. Faradaic current (A) and ionic current for mass 2 (B) measured during a potential step from 0 to −1 V (vs Ag|AgCl) in the dual thin-layer cell. Working electrode: Au; electrolyte: 0.5 M $NaClO_4$ + 10 mM $HClO_4$, saturated with CO; electrolyte flow rate: 5 μL/s. (C) Transfer efficiency calculated via eq 1 from the data shown in (A) and (B) as well as $K°(H_2)$ (Table 1). The cathode potential of the ion source of the mass spectrometer was 27.5 V.

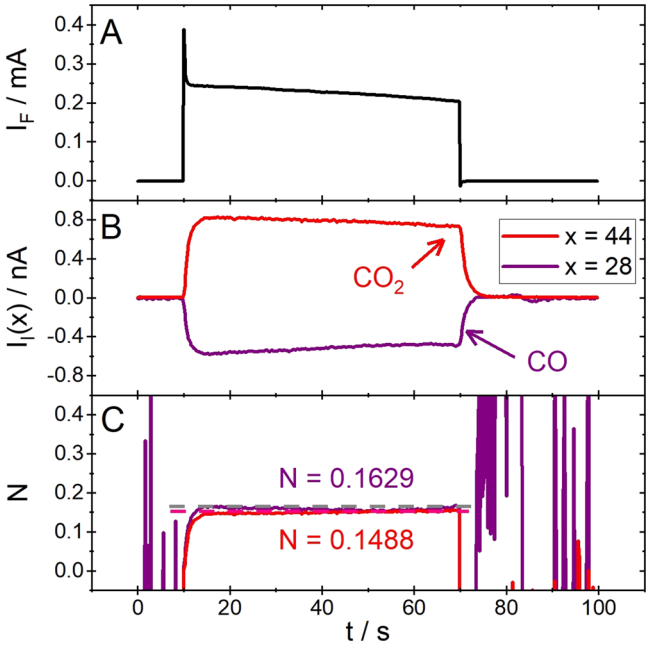

Figure 3. Faradaic current (A) and ionic current for mass 28 (black) and 44 (red) (B) measured during a potential step from 0 to 0.9 V (vs Ag|AgCl) in the dual thin-layer cell. Working electrode: Au; electrolyte: 0.5 M $NaClO_4$ + 10 mM $HClO_4$, saturated with CO; electrolyte flow rate: 5 μL/s. (C) Transfer efficiency calculated using eq 1 from the data shown in (A) and (B) as well as $K°(CO_2)$/$K°$(CO) (Table 1). The cathode potential of the ion source of the mass spectrometer was 27.5 V.

corresponding flow through experiments (Figures S1 and S2, for CO only) and the related discussion are provided in the

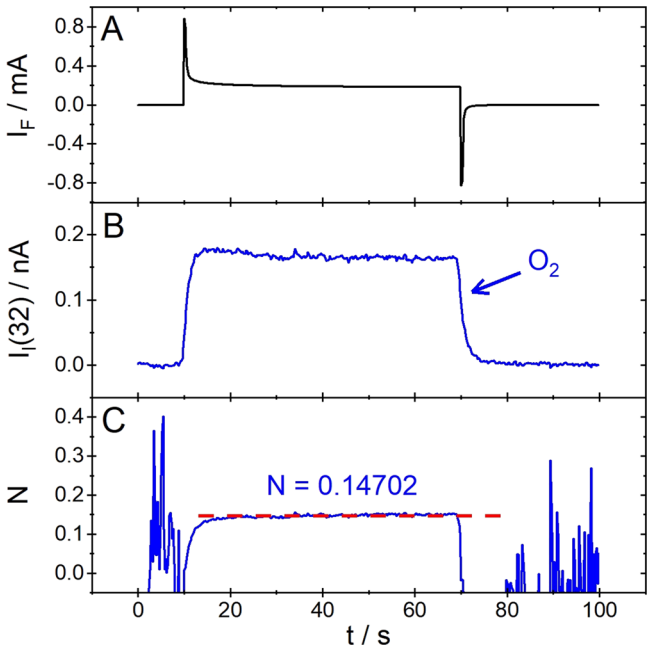

Figure 4. Faradaic current (A) and ionic current for mass 32 (B) measured during a potential step from 0 to 1.9 V (vs Ag|AgCl) in the dual thin-layer cell. Working electrode: Au; electrolyte: 0.5 M $NaClO_4$ + 10 mM $HClO_4$, saturated with CO; electrolyte flow rate: 5 μL/s. (C) Transfer efficiency calculated using eq 1 from the data shown in (A) and (B) as well as $K°(O_2)$ (Table 1). The cathode potential of the ion source of the mass spectrometer was 27.5 V.

Supporting Information. We did not determine the diffusion coefficient of CO_2 in this way, because the employed procedure involves a measurement in pure water. At this pH, CO_2 exists in equilibrium with bicarbonate, which would distort the results. Therefore, in Figure 5, the logarithm of the transfer efficiency of CO_2 is plotted against the logarithm of its diffusion coefficient in water (2.05×10^{-5} cm^2/s[22]).

Note that the plot in Figure 5 suggests an approximately linear relationship between the logarithm of the diffusion coefficient (D) and the logarithm of the transfer efficiency N. In fact, the slope of the linear fit in Figure 5 suggests that the transfer efficiency has a $D^{-1.2}$ dependency. However, the exponent with which the diffusion coefficient enters the transfer efficiency changes with each cell assembly. This becomes clear from Figure S3 of the Supporting Information, where we show the same plot as in Figure 5 for two other data sets. That is, in these data sets, N has a $D^{-0.55}$ and $D^{0.14}$ dependency, respectively. Typically, the diffusion coefficient enters with an exponent of 2/3 into equations that describe mass transport under forced convection. This is true for the Levich equation[23] and for eq S2 that describes mass transport phenomena in the dual thin-layer cell, when concentration profiles as in Scheme 1C emerge.[18,21] Considering that the situation in Scheme 1B is significantly more complex than in Scheme 1C, it is not unexpected that also a more complex relationship between D and N emerges.

Although the exact relationship between N and D remains to be identified in the future, the empirically observed relationship between the logarithm of the transfer efficiency and the logarithm of the diffusion coefficient is of great interest. This relationship allows us to employ a two-point calibration method to estimate the transfer efficiency of any compound of interest. That is, for many electrode/electrolyte systems, the

https://doi.org/10.1021/acsmeasuresciau.3c00009
ACS Meas. Sci. Au 2023, 3, 277−286

Table 1. $K°$ for H_2, O_2, CO, and CO_2 Determined via Leakage Calibration[a]

	$K°(H_2)$ [C/mol]	$K°(O_2)$ [C/mol]	$K°(CO)$ [C/mol]	$K°(CO_2)$ [C/mol]
experiment 1	1.547	2.17	2.743	4.505
experiment 2	2.747 (excluded)	2.304	2.874	4.159
experiment 3	1.574	2.441	2.831	4.662
experiment 4	1.581	2.31	2.725	4.586
average	1.568 ± 0.01	2.306 ± 0.05	2.793 ± 0.06	4.478 ± 0.1

[a]The cathode potential of the ion source of the mass spectrometer was 27.5 V.

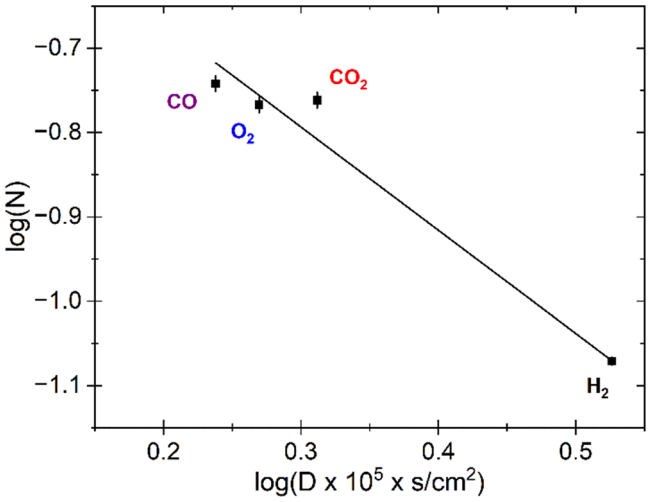

Figure 5. Plot of the logarithm of the transfer efficiency of CO, O_2, CO_2, and H_2 (from left to right) determined in Figures 2−4 versus the logarithm of the diffusion coefficient of the respective gases. Error bars due to the error of $K°$.

transfer efficiency of O_2 and H_2 is readily accessible. These two values define a straight line in the log(N) vs log(D) plot, which can be extrapolated to the diffusion coefficient of any other compound. Thus, this approach allows us to estimate the transfer efficiency of other analytes based on their respective diffusion coefficient. Once the N value is determined, leakage calibration can be conducted to determine $K°$ for the considered analyte. This allows us to employ eq 1 to quantify the mass spectrometric data and to translate them into an electrochemical product formation rate (i.e., $\frac{I_F}{z \cdot F}$).

To show that the procedure described above is a viable method to calibrate the dual thin-layer cell, we compare the transfer efficiency estimated via two-point calibration with a value that was determined experimentally. For this, we consider the electrochemical oxidation of 0.1 M 2-propanol (c.f. Scheme 2) in 0.5 M NaOH at a $Co(OH)_2/Ni(OH)_2$-codeposit electrocatalyst.

Figure 6 shows the CV and MSCV for masses 32 (oxygen) and 58 (acetone) that were collected for this electrode/electrolyte system in the potential range from 0.3 to 0.55 V.

Scheme 2. Reaction Equation of 2-Propanol Oxidation to Acetone. The Molecular Fragment of Acetone Has a Mass of 58 amu

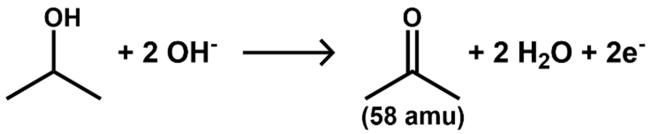

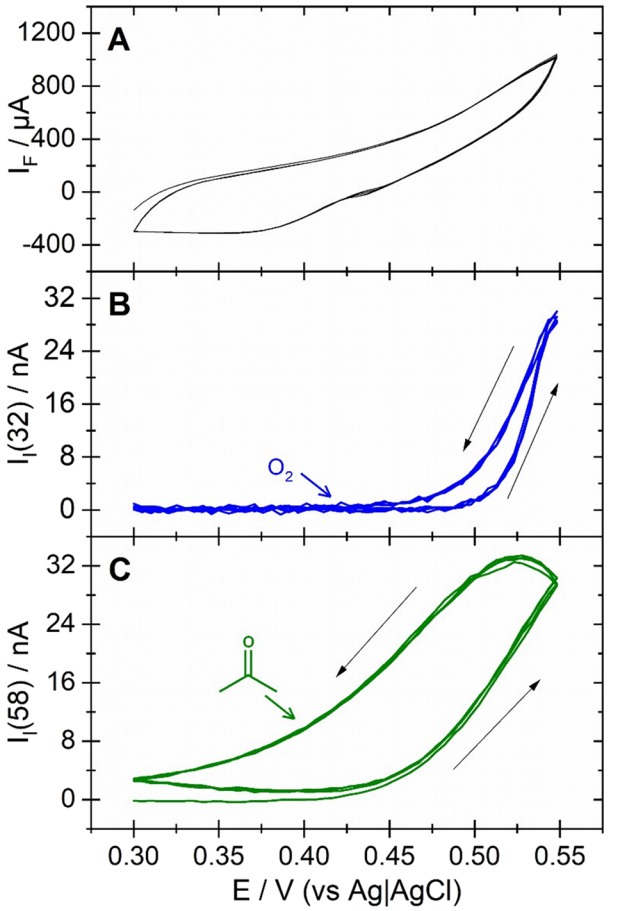

Figure 6. CV (A) and MSCVs for masses 32 (B) and 58 (C) obtained during a potential sweep from 0.3 to 0.55 V in the dual thin-layer cell. Working electrode: $Co(OH)_2/Ni(OH)_2$ codeposit on a stainless-steel electrode; electrolyte: 0.1 M 2-propanol in 0.5 M NaOH; electrolyte flow rate: 5 μL/s; sweep rate: 10 mV/s.

Due to capacitive charging, it is difficult to judge based on the CV where 2-propanol oxidation takes place. However, the evolution of a signal in the MSCV for mass 58 unambiguously indicates the formation of acetone once a potential of 0.43 V is passed in the positive-going direction. The MSCV for mass 32 indicates that the oxygen evolution reaction only occurs at potentials larger than 0.48 V. Note that both reactions retain a strong degree of hysteresis. Notwithstanding this, there is a potential region in which 2-propanol oxidation is not accompanied by the oxygen evolution reaction. Since the oxidation of secondary alcohols yields the corresponding ketone at transition metal oxides,[24] we can assume that there is a potential region in which the oxidation of 2-propanol to acetone occurs with 100% Faradaic efficiency. Hence, we can employ this reaction to determine the transfer efficiency of acetone experimentally. Furthermore, we can conduct both the

https://doi.org/10.1021/acsmeasuresciau.3c00009
ACS Meas. Sci. Au 2023, 3, 277−286

hydrogen evolution reaction and the oxygen evolution reaction to determine the transfer efficiency of H_2 and O_2, respectively. Both gases (H_2 and O_2) are evolved from the blank electrolyte to avoid overlapping signals between oxygen evolution and 2-propanol oxidation in the Faradaic current. As in the case of CO oxidation, we conduct potential step experiments to avoid an effect due to (pseudo)capacitive charging on the Faradaic current. Potential step experiments recorded in the blank electrolyte are shown in Figure 7 (steps between −1.1 and −1.41 V; hydrogen evolution) and Figure 8 (steps between 0.4 and 0.5 V, oxygen evolution). The potential step experiments conducted in the 2-propanol-containing electrolyte are shown in Figure 9 (steps between 0.3 and 0.48 V). In Figures 7−9, the Faradaic current is shown in panel A, whereas panel B shows the ionic current for the relevant mass. From the data shown in panels A and B and from the respective value of $K°$ in Table 2, we calculated the transfer efficiencies of H_2, O_2, and acetone, which are shown in panel C of Figures 7, 8 and 9, respectively. In all Figures, the value of N increases over time until it approaches a limiting value. In doing so, N mirrors behavior of the ionic current that reaches a steady value only several seconds after the potential step. We do not assign the time dependence of the ionic current to an increasing sensitivity of the filament[25] but to pseudocapacitive charging effects of the metal oxide that continue over an extended course of time. That is, as time progresses, a smaller fraction of the current is used for the chemical transformation of the metal oxide and a larger fraction of the current is used for the Faradaic reaction. Moreover, note that we observed a minor signal in the ionic current for mass 32 parallel to acetone formation (not shown in Figure 9). With the calibration constant for oxygen, determined from the experiment in Figure

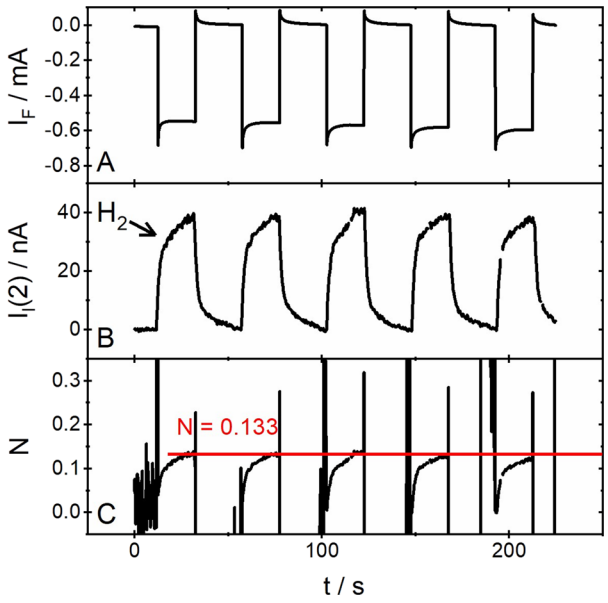

Figure 7. Faradaic current (A) and ionic current for mass 2 (B) measured during potential steps between −1.1 and −1.41 V (vs Ag|AgCl) in the dual thin-layer cell. Working electrode: $Co(OH)_2$/$Ni(OH)_2$ codeposit on a stainless-steel electrode; electrolyte: 0.5 M KOH; electrolyte flow rate: 5 μL/s. (C) Transfer efficiency calculated via eq 1 from the data shown in (A) and (B) as well as $K°(H_2)$ (Table 2). The cathode potential of the ion source of the mass spectrometer was 70 V.

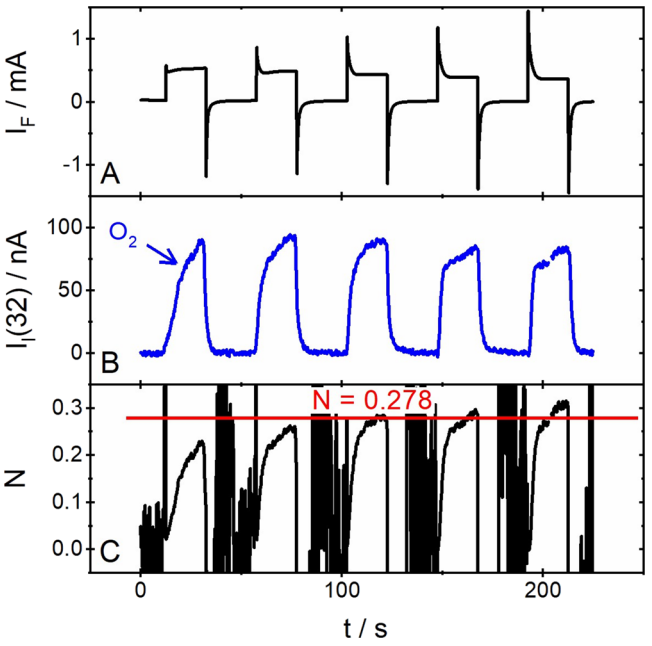

Figure 8. Faradaic current (A) and ionic current for mass 32 (B) measured during potential steps between 0.4 and 0.5 V (vs Ag|AgCl) in the dual thin-layer cell. Working electrode: $Co(OH)_2$/$Ni(OH)_2$ codeposit on a stainless-steel electrode; electrolyte: 0.5 M KOH; electrolyte flow rate: 5 μL/s. (C) Transfer efficiency calculated via eq 1 from the data shown in A and B as well as $K°(O_2)$ (Table 2). The cathode potential of the ion source of the mass spectrometer was 70 V.

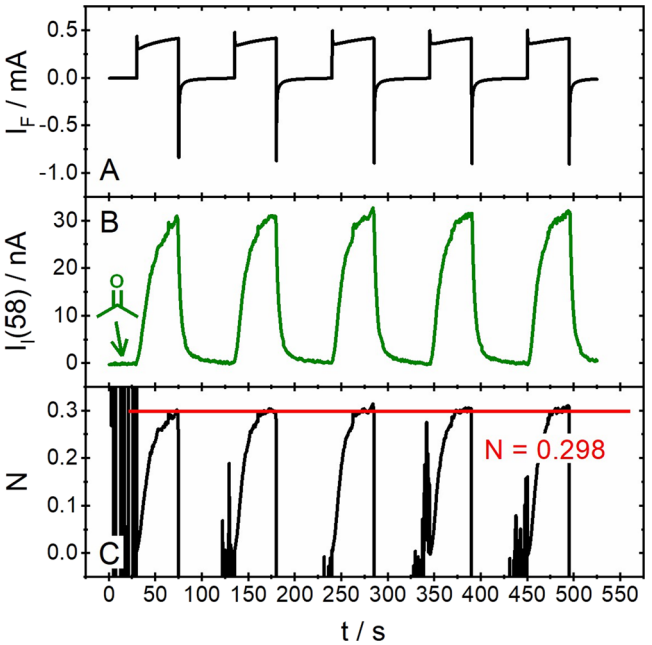

Figure 9. Faradaic current (A) and ionic current for mass 58 (B) measured during potential steps between 0.3 and 0.48 V (vs Ag|AgCl) in the dual thin-layer cell. Working electrode: $Co(OH)_2$/$Ni(OH)_2$ codeposit on a stainless-steel electrode; electrolyte: 0.1 M 2-propanol in 0.5 M KOH; electrolyte flow rate: 5 μL/s. (C) Transfer efficiency calculated via eq 1 from the data shown in A and B as well as $K°$(acetone) (Table 2). The cathode potential of the ion source of the mass spectrometer was 70 V.

https://doi.org/10.1021/acsmeasuresciau.3c00009
ACS Meas. Sci. Au 2023, 3, 277−286

Table 2. $K°$ for Acetone, O_2, and H_2 Determined via Leakage Calibration[a]

	$K°$ (acetone) [C/mol]	$K°(O_2)$ [C/mol]	$K°(H_2)$ [C/mol]
experiment 1	34.3	298.9	92.0
experiment 2	58.7	276.5	
experiment 3	46.9	278.4	109.1
experiment 4	52.0		
average	48.0 ± 4.5	284 ± 7.6	100.6 ± 6.1

[a]Cathode potential (ion source): 70 eV.

8, the ionic current for mass 32 was translated into the partial current due to oxygen evolution. The latter was subtracted from the Faradaic current shown in Figure 9, before the transfer efficiency for acetone was determined. The logarithm of the experimentally determined transfer efficiencies are plotted against the logarithm of the diffusion coefficient in Figure 10. For this plot, we used the value of N at the end of

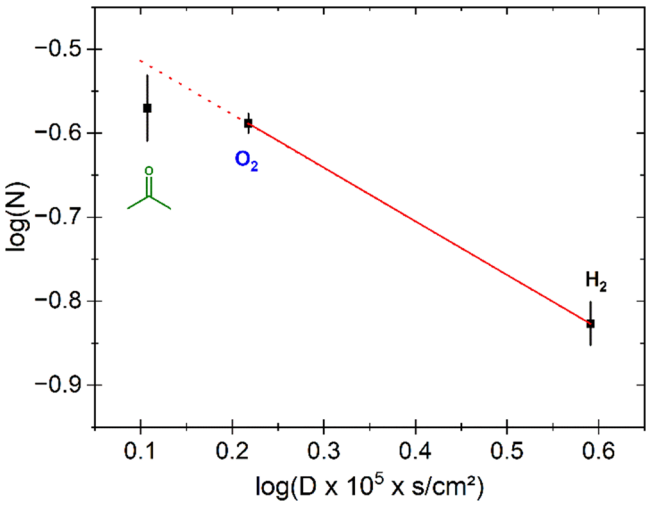

Figure 10. Plot of the transfer efficiency of acetone, O_2, and H_2 (from left to right) determined in Figures 7−9 versus the diffusion coefficient of the respective compound to the power of 4/3. Error bars due to $K°$.

the potential step to minimize the effect of pseudocapacitive charging. The diffusion coefficients of H_2 (3.9×10^{-5} cm^2/s),[26] O_2 (1.65×10^{-5} cm^2/s),[27] and acetone (1.28×10^{-5} cm^2/s)[28] were taken from literature. The straight line defined by the transfer efficiencies of hydrogen and oxygen in Figure 10 can be used to predict the transfer efficiency of acetone. From Figure 10, it is clear that the estimated and experimentally determined transfer efficiencies of acetone are in reasonable agreement. In order to explore the accuracy of the method, we have conducted the experiments of Figures 7−10 four more times and predicted the transfer efficiency of acetone from a $\log(N)$ vs $\log(D)$ plot. Table 3 compares the experimentally determined value with the values estimated from the two-point calibration method. Considering the deviation between experimentally determined and predicted values of the transfer efficiency, it appears appropriate to assume an error of about 20% on the calibration constant whenever the two-point calibration procedure is used. This allows obtaining a good estimate of the calibration constant for those cases for which other calibration procedures fail.

Table 3. Comparison of the Experimentally Determined Transfer Efficiency of Acetone with Values Determined via Two-Point Calibration

	N_{exp}	$N_{predicted}$	error [%]
experiment 1	0.232	0.262	+13
experiment 2	0.269	0.303	+13
experiment 3	0.381	0.314	−17
experiment 4	0.298	0.345	+15
experiment 5	0.315	0.409	+30

DISCUSSION

It is clear from the presented data that the logarithm of the transfer efficiency changes approximately linearly with the logarithm of the diffusion coefficient of the analyte molecule. Here, we exploit this relationship to achieve the two-point calibration of the dual thin-layer cell. To this end, we plot the logarithm of the transfer efficiency of H_2 and O_2 versus the logarithm of the diffusion coefficient. Extrapolation of the resulting straight line provides us with a good estimate of the transfer efficiency of other compounds. Multiplication of the estimated transfer efficiency with $K°$ (obtained by leakage calibration) yields the calibration constant $K*$, which can be used in combination with eq 1 to transform the signals measured with the mass spectrometer into a product formation rate. Since the transfer efficiencies of H_2 and O_2 can be determined readily in most aqueous electrolytes, the outline method poses a versatile and easy procedure to calibrate the dual thin-layer cell and should also apply for other flow cells. Furthermore, the presented results validate the previously practiced calibration procedure in which the transfer efficiency is determined for compound A and used as the transfer efficiency of compound B (provided compounds A and B have similar diffusion coefficients).[4,15] It is, however, important to note that the transfer efficiency is a function of the electrolyte flow rate.[7,20] Hence, it is necessary to conduct the described two-point calibration method with the same electrolyte flow rate as the actual electrochemical experiment. This study is limited to the use of aqueous electrolytes. However, we expect that the two-point calibration method can be employed when non-aqueous electrolytes are employed. For instance, oxygen reduction[29] and hydrogen oxidation[30] might be viable calibration reactions also in non-aqueous and aprotic electrolytes. In studies where the reaction under study is sensitive to the presence of water, calibration can be conducted after the actual experiment.

The effort of the described calibration procedure can be greatly reduced, if DEMS experiments are conducted on a regular basis: It is not necessary to determine $K°(x)$ of compound x (with x being hydrogen, oxygen, and the analyte) for each calibration experiment. Instead, we can determine $K°(x)$ for all relevant compounds once and make use of relative sensitivity factors $S^R(x)$: As outlined by eq 2, the

https://doi.org/10.1021/acsmeasuresciau.3c00009
ACS Meas. Sci. Au 2023, 3, 277−286

sensitivity of the mass spectrometer $K^{o}(x)$ is the product of the overall sensitivity of the mass spectrometer $K^{o}_{MS}(t)$ and a sensitivity factor $S(x)$, which is a molecule specific quantity.[15,19]

$$K^{o}(x, t) = S(x)\cdot K^{o}_{MS}(t) \quad (2)$$

In eq 2, $K^{o}(x, t)$ and $K^{o}_{MS}(t)$ are functions of time t as their value typically changes when the filament of the mass spectrometer ages. Note that dependence of $K^{o}(x, t)$ on the properties of analyte x is separated into $S(x)$, which is a time-independent constant for a given mass spectrometer with constant settings (e.g., insource, extraction). Although it is not possible to design an experiment that allows us to determine $K^{o}_{MS}(t)$ and $S(x)$, we can make use of eq 2, when we consider relative sensitivity factors $S^{R}(x)$. That is, we can choose one sensitivity factor and set its value arbitrarily to 1. Here, we define the relative sensitivity factor of hydrogen, $S^{R}(H_2)$, as 1, which implies the relationship given in eq 3:

$$S^{R}(H_2) = \frac{S(H_2)\cdot K^{o}_{MS}(t)}{K^{o}(H_2, t)} \quad (3)$$

All other relative sensitivity factors $S(x)$ can now be referenced to $S^{R}(H_2)$ to obtain relative sensitivity factors $S^{R}(x)$ via eq 4.

$$S^{R}(x) = \frac{S(x)}{S(H_2)} = \frac{K^{o}(x, t)}{K^{o}(H_2, t)} \quad (4)$$

Equation 4 can be employed when $K^{o}(H_2, t)$ and $K^{o}(x, t)$ were determined at the same point in time. That is, it must be made sure that any differences between $K^{o}(H_2, t)$ and $K^{o}(x, t)$ are not caused by a change of $K^{o}_{MS}(t)$ and only reflects on differences in the sensitivity factors. From the K^{o} values given in Table 2, we calculated the relative sensitivity factors that are given in Table 4. Note that the K^{o} values in Table 1 yield different relative sensitivity factors, because they were determined for a different mass spectrometer featuring different ion source settings than the values given in Table 2.

Table 4. Relative Sensitivity Factors Determined from the K^{o} Values Given in Table 2

	K^{o} [C/mol]	S^{R}
H_2	100.6 ± 6.1	1.00 ± 0.06
O_2	284.6 ± 7.6	2.83 ± 0.08
acetone	48 ± 4.5	0.48 ± 0.04

Once relative sensitivity factors are determined for a mass spectrometer, they should remain valid for an extended period of time. In order to determine the calibration constant $K^{*}(x)$ of an analyte x for a new cell setup of the dual thin-layer cell, it is then sufficient to determine the K^{*} values of hydrogen and oxygen. When the same operation as in Figure 10 is conducted with the K^{*} values divided by the respective sensitivity factor, we obtain the K^{*} value of acetone divided by its sensitivity factor. From this, we can recover the K^{*} value of acetone by multiplication with the relative sensitivity factor of acetone. Finally, this can be used in eq 1 to quantify the signal of the mass spectrometer in terms of an electrochemical product formation rate.

CONCLUSIONS

We showed in this work that the transfer efficiency of the dual thin-layer cell depends on the diffusion coefficient of the analyte molecule. This observation has been used to develop a procedure that allows us to estimate the transfer efficiency of a compound based on the transfer efficiencies for H_2 and O_2. Together with leakage calibration, this poses an easy and versatile procedure to calibrate the dual thin-layer cell and to quantify the mass spectroscopic signals in terms of product formation rates.

ASSOCIATED CONTENT

Supporting Information

The Supporting Information is available free of charge at https://pubs.acs.org/doi/10.1021/acsmeasuresciau.3c00009.

Determination of the diffusion coefficient of CO; ionic current for mass 28 (M(CO)) when CO-saturated water is flushed through the dual thin-layer cell; ionic current for mass 28 when a CO-saturated electrolyte of a solution containing 0.5 M $NaClO_4$ and 10 mM $HClO_4$ is flushed through the dual thin-layer cell; products of $c(x)$ and $K^{o}(x)$ and the product of g, $K^{o}(x)$, $c(x)$, and $D(x)^{2/3}$; plot of the logarithm of the transfer efficiencies determined in three distinct experiments for CO, O_2, CO_2, and H_2 versus the logarithm of the diffusion coefficient (PDF)

AUTHOR INFORMATION

Corresponding Author

Kristina Tschulik − *Faculty of Chemistry and Biochemistry, Laboratory of Electrochemistry & Nanoscale Materials, Ruhr-University Bochum, 44780 Bochum, Germany;* orcid.org/0000-0001-7637-4082; Email: kristina.tschulik@rub.de

Authors

Christoph J. Bondue − *Faculty of Chemistry and Biochemistry, Laboratory of Electrochemistry & Nanoscale Materials, Ruhr-University Bochum, 44780 Bochum, Germany*

Marc T. M. Koper − *Leiden Institute of Chemistry, Leiden University, 2300 RA Leiden, The Netherlands;* orcid.org/0000-0001-6777-4594

Complete contact information is available at: https://pubs.acs.org/10.1021/acsmeasuresciau.3c00009

Author Contributions

The manuscript was written through contributions of all authors. All authors have given approval to the final version of the manuscript.

Notes

The authors declare no competing financial interest.

ACKNOWLEDGMENTS

This project received funding from the European Union's Horizon 2020 research and innovation program under the Marie Skłodowska-Curie grant agreement no. 801459 - FP-RESOMUS and was funded by the Deutsche Forschungsgemeinschaft (DFG) under Germany's Excellence Strategy - EXC 2033 - 390677874 - RESOLV, the CRC 1333 - project-

ID 358283783 - SFB 1333/2 2022 and the TRR 247-388390466 (project A09).

REFERENCES

(1) de Groot, M. T.; Koper, M. T. M. The influence of nitrate concentration and acidity on the electrocatalytic reduction of nitrate on platinum. *J. Electroanal. Chem.* **2004**, *562*, 81−94.

(2) Bondue, C. J.; Graf, M.; Goyal, A.; Koper, M. T. M. Suppression of Hydrogen Evolution in Acidic Electrolytes by Electrochemical CO_2 Reduction. *J. Am. Chem. Soc.* **2021**, *143*, 279−285.

(3) Schmidt, V. M.; Pastor, E. Adsorption and oxidation of acetylene and ethylene on gold electrodes. *J. Electroanal. Chem.* **1994**, *376*, 65−72.

(4) Bondue, C. J.; Koper, M. T. M. A DEMS approach for the direct detection of CO formed during electrochemical CO_2 reduction. *J. Electroanal. Chem.* **2020**, *875*, No. 113842.

(5) Trimarco, D. B.; Pedersen, T.; Hansen, O.; Chorkendorff, I.; Vesborg, P. C. K. Fast and sensitive method for detecting volatile species in liquids. *Rev. Sci. Instrum.* **2015**, *86*, No. 075006.

(6) Jusys, Z.; Massong, H.; Baltruschat, H. A New Approach for Simultaneous DEMS and EQCM: Electro-oxidation of Adsorbed CO on Pt and Pt-Ru. *J. Electrochem. Soc.* **1999**, *146*, 1093−1098.

(7) Baltruschat, H. Differential electrochemical mass spectrometry. *J. Am. Soc. Mass Spectrom.* **2004**, *15*, 1693−1706.

(8) Ashton, S. J. *Design, Construction and Research Application of a Differential Electrochemical Mass Spectrometer (DEMS)*; SpringerLink Bücher, Vol. *8*; Springer, 2012, DOI: 10.1007/978-3-642-30550-4.

(9) Clark, E. L.; Singh, M. R.; Kwon, Y.; Bell, A. T. Differential Electrochemical Mass Spectrometer Cell Design for Online Quantification of Products Produced during Electrochemical Reduction of CO_2. *Anal. Chem.* **2015**, *87*, 8013−8020.

(10) Möller, S.; Barwe, S.; Masa, J.; Wintrich, D.; Seisel, S.; Baltruschat, H.; Schuhmann, W. Online Monitoring of Electrochemical Carbon Corrosion in Alkaline Electrolytes by Differential Electrochemical Mass Spectrometry. *Angew. Chem., Int. Ed.* **2020**, *59*, 1585−1589.

(11) Bondue, C. J.; Königshoven, P.; Baltruschat, H. A New 2-Compartment Flow Through Cell for the Simultaneous Detection of Electrochemical Reaction Products by a Detection Electrode and Mass Spectroscopy. *Electrochim. Acta* **2016**, *214*, 241−252.

(12) Abd-El-Latif, A. A.; Bondue, C. J.; Ernst, S.; Hegemann, M.; Kaul, J. K.; Khodayari, M.; Mostafa, E.; Stefanova, A.; Baltruschat, H. Insights into electrochemical reactions by differential electrochemical mass spectrometry. *TrAC, Trends Anal. Chem.* **2015**, *70*, 4−13.

(13) Abd-El-Latif, A.-E.-A. A.; Xu, J.; Bogolowski, N.; Königshoven, P.; Baltruschat, H. New Cell for DEMS Applicable to Different Electrode Sizes. *Electrocatalysis* **2012**, *3*, 39−47.

(14) Wang, X.; de Araújo, J. F.; Ju, W.; Bagger, A.; Schmies, H.; Kühl, S.; Rossmeisl, J.; Strasser, P. Mechanistic reaction pathways of enhanced ethylene yields during electroreduction of CO_2-CO co-feeds on Cu and Cu-tandem electrocatalysts. *Nat. Nanotechnol.* **2019**, *14*, 1063−1070.

(15) Ferreira de Araújo, J. V. Differential electrochemical mass spectrometry − design, set up and application for kinetic isotope labeling studies of the electrocatalytic CO2 electroreduction; Doctoral Thesis, Technische Universität: Berlin, Berlin, 2020, DOI: 10.14279/depositonce-9932.

(16) Sun, S.; Xu, Z. J. Composition dependence of methanol oxidation activity in nickel−cobalt hydroxides and oxides: an optimization toward highly active electrodes. *Electrochim. Acta* **2015**, *165*, 56−66.

(17) Wolter, O.; Heitbaum, J. Differential Electrochemical Mass Spectroscopy (DEMS) - a New Method for the Study of Electrode Processes. *Ber. Bunsen-Ges. Phys. Chem.* **1984**, *88*, 2−6.

(18) Merdon, C.; Fuhrmann, J.; Linke, A.; Streckenbach, T.; Neumann, F.; Khodayari, M.; Baltruschat, H. Inverse modeling of thin layer flow cells for detection of solubility, transport and reaction coefficients from experimental data. *Electrochim. Acta* **2016**, *211*, 1−10.

(19) Löffler, T. Der Einfluss monoatomarer Stufen und der Temperatur auf die Adsorption und Hydrierung ungesättigter organischer Verbindungen; Doctoral Thesis, Rheinische Friedrich-Wilhelms Universität Bonn, Bonn, 2003.

(20) Chen, W.; Uwitonze, N.; He, F.; Sartin, M. M.; Cai, J.; Chen, Y.-X. Effect of mass transfer and solution composition on the quantification of reaction kinetics by differential electrochemical mass spectrometry. *J. Energy Chem.* **2021**, *56*, 412−419.

(21) Khodayari, M.; Reinsberg, P.; Abd-El-Latif, A.-E.-A. A.; Merdon, C.; Fuhrmann, J.; Baltruschat, H. Determining Solubility and Diffusivity by Using a Flow Cell Coupled to a Mass Spectrometer. *ChemPhysChem* **2016**, *17*, 1647−1655.

(22) Hawke, J. G.; White, I. Temperature dependence of the diffusion coefficient of carbon-14 dioxide in dilute hydrochloric acid. *J. Phys. Chem.* **1975**, *79*, 1614−1617.

(23) Bard, A. J.; Faulkner, L. R. *Electrochemical methods:Fundamentals and applications*; 2 ed.; Wiley, 2001.

(24) Schäfer, H.-J. Oxidation of organic compounds at the nickel hydroxide electrode. In *Electrochemistry I*; Dewar, M. J. S.; Dunitz, J. D.; Hafner, K.; Heilbronner, E.; Itô, S.; Lehn, J.-M.; Niedenzu, K.; Raymond, K. N.; Rees, C. W.; Vögtle, F.; Wittig, G.; Steckhan, E., Eds.; Topics in Current Chemistry; Springer Berlin Heidelberg, 1987; pp. 101−129, DOI: 10.1007/3-540-17871-6_13.

(25) He, F.; Chen, W.; Chen, J.-Q.; Zhen, E.-F.; Cai, J.; Chen, Y.-X. The Effect of Water on the Quantification of Volatile Species by Differential Electrochemical Mass Spectrometry. *Anal. Chem.* **2021**, *93*, 5547−5555. Published Online: Mar. 22, 2021

(26) Rüetschi, P. Solubility and Diffusion of Hydrogen in Strong Electrolytes and the Generation and Consumption of Hydrogen in Sealed Primary Batteries. *J. Electrochem. Soc.* **1967**, *114*, 301−305.

(27) Davis, R. E.; Horvath, G. L.; Tobias, C. W. The solubility and diffusion coefficient of oxygen in potassium hydroxide solutions. *Electrochim. Acta* **1967**, *12*, 287−297.

(28) Yaws, C. L. Diffusion Coefficient in Water − Organic Compounds. In *Transport Properties of Chemicals and Hydrocarbons*; Elsevier, 2009; pp. 502−593, DOI: 10.1016/B978-0-8155-2039-9.50017-X.

(29) Bondue, C. J.; Reinsberg, P.; Abd-El-Latif, A. A.; Baltruschat, H. Oxygen reduction and oxygen evolution in DMSO based electrolytes: the role of the electrocatalyst. *PCCP Phys. Chem. Chem. Phys.* **2015**, *17*, 25593−25606.

(30) Ledezma-Yanez, I.; Díaz-Morales, O.; Figueiredo, M. C.; Koper, M. T. M. Hydrogen Oxidation and Hydrogen Evolution on a Platinum Electrode in Acetonitrile. *ChemElectroChem* **2015**, *2*, 1612−1622.

https://doi.org/10.1021/acsmeasuresciau.3c00009
ACS Meas. Sci. Au 2023, 3, 277−286